Marine Geology xxx (2009) xxx–xxx

Contents lists available at ScienceDirect

Marine Geology

journal homepage: www.elsevier.com/locate/margeo

Testing proposed mechanisms for seafloor weakening at the top of gas hydrate stability on an uplifted submarine ridge (Rock Garden), New Zealand

S. Ellis [a,*], I. Pecher [a,b], N. Kukowski [c], W. Xu [d], S. Henrys [a], J. Greinert [e,f]

[a] GNS Science, PO Box 30-368, 1 Fairway Drive, Lower Hutt, New Zealand
[b] Inst. of Petroleum Engineering, Heriot-Watt Univ., Edinburgh, EH3 9HP, UK
[c] GFZ Potsdam Telegrafenberg 14473 Potsdam, Germany
[d] RTC - Unconventional Gas- Schlumberger, 14131 Midway Rd, suite 700, Addison, TX 75001, USA
[e] Renard Centre of Marine Geology (RCMG), Ghent University, Krijgslaan 281 s8, B-9000 Gent, Belgium
[f] Royal Netherlands Institute for Sea Research (NIOZ), PO Box 59, 1790 AB, Den Burg (Texel), The Netherlands

ARTICLE INFO

Article history:
Received 4 August 2008
Received in revised form 26 August 2009
Accepted 5 October 2009
Available online xxxx

Keywords:
gas hydrates
seafloor erosion
stability
dissociation
overpressure
uplift

ABSTRACT

We evaluate different hypotheses concerning the formation of a peculiar, flat-topped ridge at Rock Garden, offshore of the North Island of New Zealand. The coincidence of the ridge bathymetry with the depth at which gas hydrate stability intersects the seafloor has been previously used to propose that processes at the top of gas hydrate stability may cause seafloor erosion, giving rise to the flat ridge morphology. Two mechanisms that lead to increased fluid pressure (and sediment weakening) have previously been proposed: (1) periodic formation (association) and dissociation of gas hydrates during seafloor temperature fluctuations; and (2) dissociation of gas hydrates at the base of gas hydrate stability during ridge uplift. We use numerical models to test these hypotheses, as well as to evaluate whether the ridge morphology can develop by tectonic deformation during subduction of a seamount, without any involvement from gas hydrates. We apply a commonly-used 1D approach to model gas hydrate formation and dissociation, and develop a 2D mechanical model to evaluate tectonic deformation. Our results indicate that: (1) Tectonics (subduction of a seamount) may cause a temporary flat ridge morphology to develop, but this evolves over time and is unlikely to provide the main explanation for the ridge morphology; (2) Where high methane flux overwhelms the anaerobic oxidation of methane via sulphate reduction near the seafloor, short-period temperature fluctuations (but on timescales of years, not months as proposed originally) in the bottom water can lead to periodic association and dissociation of a small percentage of gas hydrate in the top of the sediment column. However, the effect of this on sediment strength is likely to be small, as evidenced by the negligible change in computed effective pressure; (3) The most likely mechanism to cause sediment weakening, leading to seafloor erosion, results from the interaction of gas hydrate stability with tectonic uplift of the ridge, provided bulk permeability strongly decreases with increasing hydrate content. Rather than overpressure developing from dissociation of hydrates at the base of gas hydrate stability (as previously thought), we found that the weakening is caused by focusing of gas hydrate formation at shallow sediment levels. This creates large fluid pressures and can lead to negative effective pressures near the seafloor, reducing the sediment strength.

1. Introduction

Formation (association) of methane gas hydrate beneath the seafloor is limited by the range in temperature and pressure at which gas hydrate is stable, and also by the available supply of methane and water (e.g., Rempel and Buffett, 1997; Sloan, 1998; Xu and Ruppel, 1999). Over time, gas hydrate zones can shrink or expand as local pressure, temperature, and methane supply changes (e.g., Sultan et al., 2004). Such variations are thought to have significant effects on physical properties of sediment. For example, overpressure generated from volume expansion during dissociation of hydrate to gas and water may lead to sediment weakening at the base of the gas hydrate stability zone and possibly trigger submarine slope failure (Mienert et al., 1998, 2005; Xu and Germanovich, 2006). Conversely, several laboratory studies have shown that the presence of gas hydrate in the pore space increases sediment strength (Yun et al., 2007; Winters et al., 2007).

In this paper, we investigate a possible link between gas hydrate dissociation and sediment strength along the Hikurangi Margin of New Zealand (Fig. 1). The central part of the Hikurangi Margin of New Zealand is characterised by a series of long (<100 km), sub-parallel accretionary ridges (Barnes and Mercier de Lépinay, 1997). Along part of this margin, in contrast to the usual ridge morphology, some ridges have

* Corresponding author. Tel.: +64 4 570 4730; fax: +64 4 570 4600.
E-mail addresses: s.ellis@gns.cri.nz (S. Ellis), i.pecher@gns.cri.nz (I. Pecher), nina.kukowski@gfz-potsdam.de (N. Kukowski).

0025-3227/$ – see front matter © 2009 Elsevier B.V. All rights reserved.
doi:10.1016/j.margeo.2009.10.008

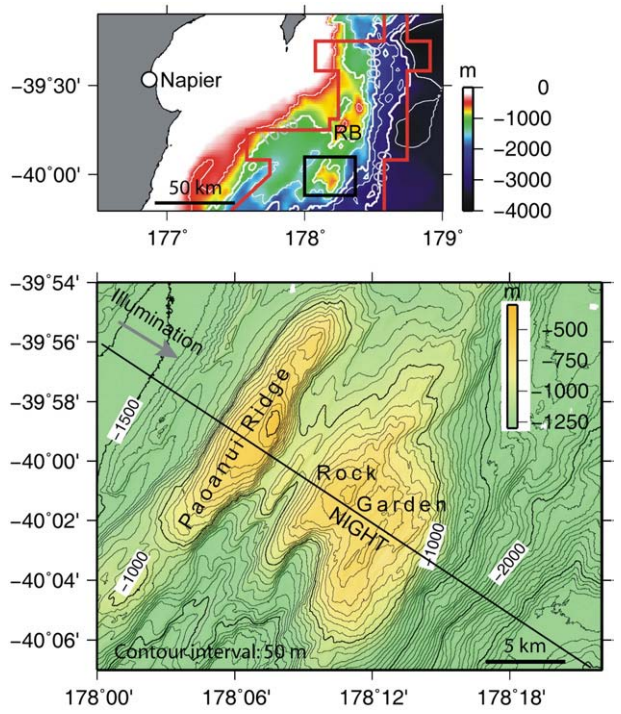

Fig. 1. Tectonic setting (top) and location of Ritchie Ridge and Rock Garden (outlined in black box at top), offshore North Island, New Zealand, modified from Pecher et al. (2005). RB = North Island Geophysical Transect. The area enclosed by red lines (top) shows the approximate extent of bottom simulating reflectors (BSRs) representing the base of the gas hydrate stability field. BSRs are prevalent along most of the East Coast margin in water depths ranging from 600 to 3000 m (Henrys et al., 2003b). (For interpretation of the references to colour in this figure legend, the reader is referred to the web version of this article.)

a several-kilometre wide flat top. The observation of pinch-outs of bottom simulating reflectors (BSRs) at the edges of the flat-topped ridges led Pecher et al. (2005) to suggest a mechanism of gas-hydrate-related seafloor erosion. Two processes were proposed (Fig. 2): (1) During ridge uplift, an upward migrating base of gas hydrate stability (BGHS) with respect to the seafloor may lead to gas hydrate dissociation, overpressure, seafloor weakening, and ultimately, slope failure. After sliding, water depth, and hence hydrate stability, increase again and the process may repeat itself during continued uplift. Evidence from bathymetric and seismic data supports the presence of small slides on the edges of the plateau; (2) Repeated dissociation and formation of gas hydrates on the ridge crests caused by water temperature fluctuations may contribute to seafloor weakening. During warm-water periods, gas hydrates can dissociate, leading to net pore-volume expansion, whereas pore volume can contract during gas hydrate formation in cold-water periods. It was hypothesized that repeated pore-volume contraction and expansion could cause weakening of the seafloor. Weakened sediments would then slide down the steep ridge flanks and/or be eroded by water currents. It was known that water temperatures in the study area varied by at least ± 0.9 °C. Hence, the top of the gas hydrate stability in the ocean was predicted to repeatedly move up and down by ± 35 m. In other words, the seafloor around the BSR pinch-outs was predicted to repeatedly enter and leave the gas hydrate stability field, so that any gas hydrate close to the seafloor would repeatedly form and dissociate. Meso-scale (100–200-day) variations of the Wairarapa Eddy were suggested to be the most likely cause for the temperature changes.

As pointed out by Pecher et al. (2005), several parts of the proposed gas-hydrate-related weakening mechanisms need to be verified. Dissociation of gas hydrates at the BGHS requires that the ridges need to remain within the gas hydrate stability field (for the average bottom-water temperature), which seems to contradict the presence of BSR pinch-outs. For repeated dissociation of gas hydrates to cause weakening, the thermal signal needs to reach the depths of gas-hydrate-bearing layers, which may not reach the seafloor owing to oxidation at the sulphate–methane interface (Borowski et al., 1996).

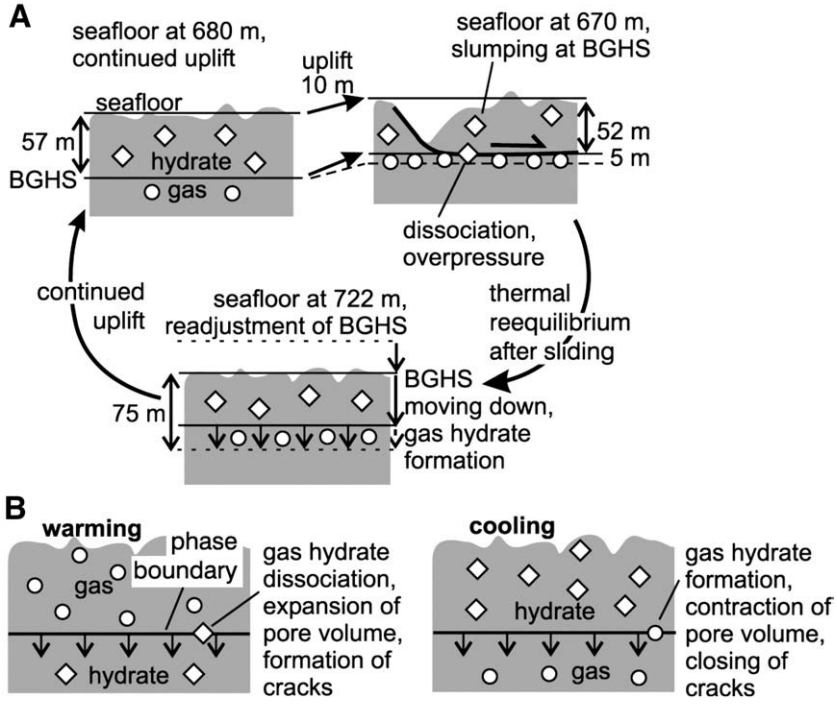

Fig. 2. Conceptual models proposed by Pecher et al. (2005) for the weakening of surface sediment caused by interaction with hydrate formation/dissociation. (A) Gas hydrate dissociation during uplift of the ridge causes overpressure and mechanical weakening at the bottom of gas hydrate stability, inducing mass failure and slumping; (B) Repeated formation and dissociation of hydrate during seafloor warming and cooling cycles weaken the seafloor.

Please cite this article as: Ellis, S., et al., Testing proposed mechanisms for seafloor weakening at the top of gas hydrate stability on an uplifted submarine ridge (Rock Garden), New Zealand, Marine Geology (2009), doi:10.1016/j.margeo.2009.10.008

In addition to Rock Garden, two ridges further to the north — the western-most and possibly, the eastern-most ridges of Ritchie Banks — display a similar flattened ridge top flanked by BSR pinch-outs. Hence, erosion at these depths must be linked to a regional mechanism. Regional uplift, sub-aerial and/or wave erosion, followed by subsidence to current depths, was considered unlikely by Pecher et al. (2005) because of the smooth flanks of another ridge that crosses the ~600 m water depth. If this mechanism were responsible for ridge morphology, regional uplift should have exposed this ridge to sub-aerial erosion, and hence a change in slope dip would be expected. Likewise, current erosion above ~600 m water depth (as an alternative regional erosion mechanism) would also affect this ridge, leading to a change in slope dip which is not observed. This suggests that although currents may ultimately be responsible for erosion at Rock Garden, their efficacy must be enhanced by some process that weakens near-seafloor sediments.

Rock Garden is thought to be uplifted by a subducting seamount (Henrys et al., 2006; Barnes et al., 2009-this issue). Recently, the shape of this seamount has been constrained more accurately. Depth conversions using wide-angle velocity data indicate the top of the seamount to be ~5 km beneath the seafloor and stand approximately 3 km above the subducting Hikurangi Plateau (Fig. 3B). This enables us to test whether Rock Garden ridge morphology results from the subducting seamount and not from the interaction with gas hydrates in the sediment at all. We note that it would be a coincidence if this mechanism also applies to shape the western-most Ritchie Banks ridge.

In this paper, we use numerical models to evaluate the proposed mechanisms for creation of the flat-topped ridges of Rock Garden. A one-dimensional model of fluid flow and transport of heat, methane, and salt in a porous medium is used (Xu, 2004) to simulate the effects of uplift and of a small-scale temperature fluctuation at the seafloor on gas hydrate formation, dissolution, and dissociation. We constrain uplift rates using a 2D mechanical model. These models, together with a review of tectonic and methane constraints from data collected on and around Rock Garden and Ritchie Ridge, are used to evaluate whether either of the following hypotheses is a plausible explanation for the ridge morphology:

Hypothesis 1. A consequence of tectonics only (subduction of a seamount or lower plate high), so that the correspondence between a flat bathymetry and the predicted depth of BSR pinch-outs is purely coincidental;

Hypothesis 2. Caused by mechanical strength changes owing to interaction of sediment with gas hydrates, either by:

a. Repeated formation and dissociation of hydrates near the seafloor as a result of temperature changes; or
b. Dissociation of gas hydrates at the base of the gas hydrate stability zone resulting from tectonic uplift.

For Hypothesis 2, we assume that once sediment is mechanically weakened, it is then eroded by bottom currents and/or internal waves, creating flat-topped ridges by submarine erosion (e.g., Cacchione et al., 2002).

2. Data constraints

Along the Hikurangi subduction margin, North Island New Zealand, the oblique subduction of Pacific oceanic lithosphere beneath continental Australian plate lithosphere has created a series of uplifted anticlines within the offshore accretionary wedge (Figs. 1 and 3; Davey et al., 1986; Barnes and Mercier de Lépinay, 1997; Henrys et al., 2003a). While the accretionary morphology along the southern part of this margin is thought to be entirely controlled by thrusting, seamount subduction is inferred to generate uplift in the central part of the margin (Barnes et al., 2009 — this issue) with Rock Garden being the southern-most seamount-related ridge.

Observations from this area relevant to our tests include:

- Steep slopes of Rock Garden have been interpreted to indicate that overconsolidated material is being exhumed there (Pecher et al., 2005). This interpretation was confirmed by the recovery of consolidated rocks in dredge samples — mainly fractured mudstone, but also some inundated sandstone, as well as carbonates (Pecher et al., 2007).
- A temperature probe was recovered from 580 m water depth on Ritchie Banks in 2006 (Pecher et al., 2007; Pecher et al., 2008), indicating that temperatures were ~0.5 °C lower than the lowest temperatures predicted by Pecher et al. (2005) based on historic CTD data. It also appeared that the period of the temperature fluctuations was longer than the 15-month deployment (Pecher

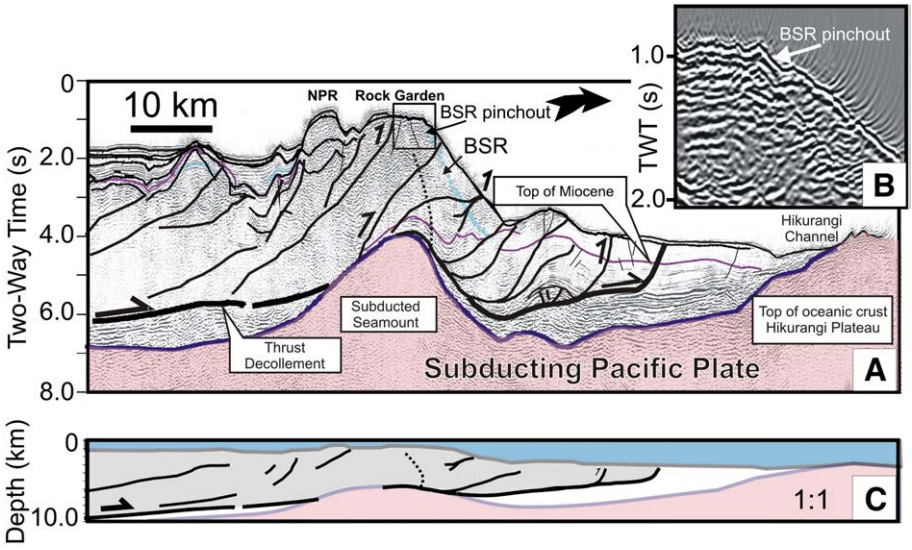

Fig. 3. Multichannel seismic sections across the Rock Garden bathymetric high. NIGHT profile locations are shown in Fig. 1. Eastern part of NIGHT seismic data acquired by M/V Geco Resolution across the Hawke Bay margin (Henrys et al., 2003a). Upper margin structures are correlated to and mapped with an extensive set of high-quality industry and research seismic sections (Barnes et al., 2009 — this issue). Active thrust faults are shown in bold. NPR, northern Paoanui Ridge; BSR is shown in the dashed blue line and pinches out near the summit of Rock Garden. (B) Enlarged portion of seismic section of BSR pinch out on the summit of Rock Garden. (C) Depth converted seismic section using velocities derived from wide-angle reflection data and shown without vertical exaggeration. (For interpretation of the references to colour in this figure legend, the reader is referred to the web version of this article.)

Please cite this article as: Ellis, S., et al., Testing proposed mechanisms for seafloor weakening at the top of gas hydrate stability on an uplifted submarine ridge (Rock Garden), New Zealand, Marine Geology (2009), doi:10.1016/j.margeo.2009.10.008

et al., 2008). This suggests a timescale of >2 years and a greater temperature fluctuation (±1.2 °C) than that inferred by Pecher et al. (2005).

- Strong bottom currents are thought to be present that should be capable of eroding weakened, loose sediment (current speeds averaging ca. 0.2 ms^{-1} have been measured at ~200 m depth, although no direct measurements exist for Rock Garden; Chiswell, pers. comm.; Faure et al., 2009 — this issue).
- Seep sites have been discovered where methane bubbles rise into the water column (Faure and Greinert, 2006; Faure et al., 2009 — this issue). Together with the presence of gas hydrates in the top centimetres of the seafloor, this suggests that at some locations, the sulphate reduction zone (where methane is consumed near the seafloor) is shallow and/or by-passed by (fault) focused fluids, and that methane concentrations at the top of the sediment column may be significant (cf. Borowski et al., 1996, 1999; Borowski, 2004), although even at seep sites the methane is undersaturated in seawater.
- ROV and video grab images of seep sites reveal numerous ancient seeps that are no longer active, suggesting that gas is released in transient bursts rather than concurrently over the entire seep area. Some of the seeps span a large surface area, of up to half a square kilometre (Naudts et al., this issue).
- Free gas layers that approach the seafloor, in particular beneath seep sites, have been imaged on high-resolution seismic profiles (Crutchley et al., 2009 — this issue).
- A preliminary analysis of gas at seeps at Rock Garden and other east coast sites suggests that they are almost 100% biogenic methane by composition, with source methane having $\delta^{13}C_{CH4}$ values of −68 to −66% and an absence of higher hydrocarbons in most of the samples (Faure et al., 2009 — this issue).

3. Hypothesis 1: is ridge morphology caused by tectonics?

The ridge at Rock Garden is flatter than similar structures along the Hikurangi Margin (Barnes et al., 2009 — this issue). Subduction of seamounts at other convergent margins causes a wide variety of deformation styles, depending on the material composition of the over-riding plate (Lallemand et al., 1989; von Huene et al., 1997; Dominguez et al., 1998; Kobayashi et al., 1998; Park et al., 1999). Seamount subduction has affected the style of deformation at the trench front and within the accretionary prism along the East Coast margin of New Zealand, causing tectonic erosion and indentation (Collot et al., 2001; Lewis et al., 2004). Assuming a convergent velocity of ca. 4 cm yr^{-1}, the seamount would have encountered the accretionary prism about 1.3 Ma, and so is expected to have had a major influence on ridge development during that period of time.

To test whether the flat ridge morphology can result from subduction of a seamount or equivalent basement high, a two-dimensional mechanical finite-element model has been developed, which models frictional plastic flow based on a Coulomb yield criterion, and allows large strain to develop by tracking strain and other quantities on tracer particles (Fullsack, 1995; Moresi et al., 2003; Smith and Griffiths, 2004). The initial conditions are shown in Fig. 4A. Velocity boundary conditions of 4 cm yr^{-1} are applied at the sides and base of the model to simulate low-angle subduction. Material frictional strength is a function of effective pressure and sediment type (Table 1). The prescribed geometry of the subduction interface warps upward with a width of 40 km and height of 3 km to represent the basement high (seamount). The subduction interface is prescribed as a continuous, low-strength layer; this may result from fluid overpressuring, though here it is represented with a lower angle of internal friction (Table 1).

Fig. 4B–D shows how the seamount localizes frictional deformation (as measured by the amount of strain softening in the sediment), while at the same time an accretionary wedge with a shallow slope of ca. 4° develops against the backstop (to the left of the seamount). Because material moves from right to left, there is a superposition in deformation style. Initially, material above the leading edge of the subducting seamount is uplifted and sheared. Once the seamount passes below it, subsidence and normal faulting occur (Fig. 4E). The pattern shown in the simple numerical model is similar to that described from sandbox experiments by Dominguez et al. (2000), but the model shown here is approximately scaled to the dimensions of the Hikurangi subduction margin. The model also demonstrates how locally "flat" morphology can develop. For example, in the early stages of deformation (Fig. 4B), a wide uplifted step with low relief is present to the left of the seamount (indicated by the horizontal bar above the figure). Later on, the bathymetry becomes tilted and the flat zone is substantially reduced in width, with tilting of the surface and development of slopes exceeding 10° (Fig. 4C–D). The model result suggests that flat areas can be present merely as a result of tectonics, but that these flat regions are short-lived, and become less pronounced with continued subduction of the seamount. The present morphology of Rock Garden (Fig. 3B) is closest to the deformation shown in Fig. 4C (i.e. ca. 1 My since the seamount was under the toe of the wedge), where the seamount is at a depth of ca. 5 km below the seafloor, and seaward-verging faults have developed. For this model stage, "flat" bathymetry (defined as having a slope of <1°) occurs over a width of about 7 km.

The uplift shown in Fig. 4B–D occurs slightly landward of the seamount. This is because the seamount is pushing landward on the overlying sediment, as well as displacing it upward (Fig. 4E). In comparison, the morphology shown in Fig. 3C suggests uplift directly above the inferred location of the seamount high. Numerical sensitivity tests show that a more symmetric uplift above the seamount can be obtained if the weak subduction interface material is not present above the seamount (Fig. 4F). In this case, uplift rates above the seamount are slightly higher, and a strongly deforming fault is predicted to form seaward of the uplifted region, with a locally flat, ~12 km-wide uplifted region above the seamount.

Fig. 4E also plots vertical uplift velocity at the surface after a 1 My deformation. Uplift rates above the leading edge of the seamount are initially high, but fall off over time, as the seamount moves landward, with subsidence in its wake and accompanying tilting of the initially uplifted plug above it. During the period where a particular point on the surface enters the constructive (uplift) phase on the landward side of the seamount, the average uplift velocity is about 5 mm yr^{-1}. The constructive phase for a given point on the surface lasts for about 0.5 My, which is roughly the time taken for half of the width of the seamount to advect beneath it. This gives a total uplift of ca. 2.5 km (note that total relief after 1 My is more than this, e.g., Fig. 4C, because at the same time the surface on the seaward side is subsiding with the subducting plate).

The morphology of the ridge in the simple 2D numerical model depends partly on how localized deformation is on bounding faults. The case shown in Fig. 4B–E develops faults (localized shearing zones) which allow uplift of material between them with low relief, although this becomes narrower and more tilted with increasing deformation. Sensitivity studies show that the more localized the deformation, the broader the zone of low relief, in which case no interplay with hydrates would be needed to explain the ridge morphology. However, seismic interpretations suggest a distributed series of faults rather than only 1–2 strongly localized faults above the subducting seamount at Rock Garden (Fig. 3A; Barnes et al., 2009 — this issue). Also, the association of flat-topped ridges with BSRs, while a nearby ridge with no BSR present has been uplifted through the 600 m depth with no change in slope (Pecher et al., 2005, 2008), supports a mechanism by which a change in upper ridge sediment strength (via interaction with hydrates) can explain the flat-topped nature, although the numerical models shown here suggest that short-lived zones with low relief (slopes of less than 1°) can be at least partly explained by tectonics.

Please cite this article as: Ellis, S., et al., Testing proposed mechanisms for seafloor weakening at the top of gas hydrate stability on an uplifted submarine ridge (Rock Garden), New Zealand, Marine Geology (2009), doi:10.1016/j.margeo.2009.10.008

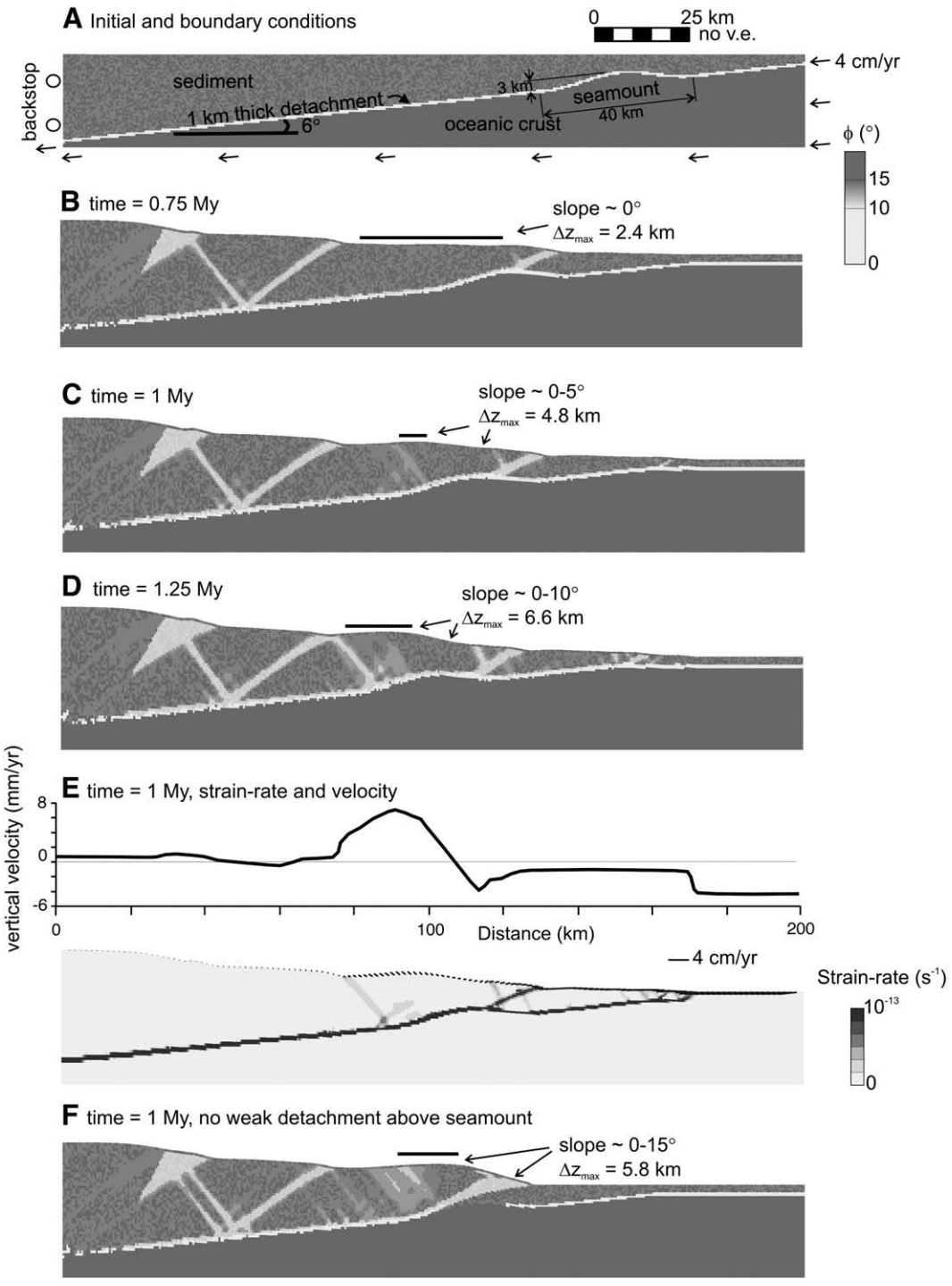

Fig. 4. Mechanical model of seamount subduction. (A) Initial and boundary conditions. No vertical exaggeration. Seamount is represented by a 40-km-wide swell (3-km high) entering from the left. Subduction velocity is 4 cm yr^{-1}. A weak frictional detachment, 1 km thick, dips at an angle of 6°. Greyscales show internal angle of friction, ϕ (see also Table 1). (B–D) Evolution in frictional strength after 0.75–1.25 My. An accretionary wedge forms against the backstop, and the seamount acts to focus toe deformation. Black thick line shows extent of "flat zone" above and to right of subducting seamount. Slope and change in bathymetry cf. the left-hand edge of the model are also indicated. (E) Profile of uplift across-strike (top) and second invariant of the strain-rate tensor (grey scales, bottom) with surface velocity superimposed as a vector plot, showing focusing effect of the seamount, and a change from subduction to uplift as the seamount subducts underneath. (F) Same as (C) but for a model that has no detachment layer on top of the seamount.

4. Hypothesis 2: is ridge morphology controlled by sediment strength changes from gas hydrate evolution?

To investigate whether mechanical weakening of sediment can be caused by changes in gas hydrate stability, we have conducted numerical experiments using a one-dimensional, three-phase finite-difference code that predicts fluid flow, transport of heat, methane, and salt in a porous medium (Fig. 5; see Xu, 2004 for details). We considered model behaviour under a range of conditions, starting from the simplest — a uniform depth, seafloor temperature, and methane flux — and progressing to a more realistic setting that incorporates cyclical changes in bottom-water temperature, and gradual uplift causing a pressure reduction, based on uplift rates inferred from the mechanical models of seamount behaviour.

Please cite this article as: Ellis, S., et al., Testing proposed mechanisms for seafloor weakening at the top of gas hydrate stability on an uplifted submarine ridge (Rock Garden), New Zealand, Marine Geology (2009), doi:10.1016/j.margeo.2009.10.008

Table 1
Frictional properties used in the 2D mechanical model.

	Peak and softened angles of internal friction[a]	Finite strains over which friction angle linearly decreases	Cohesion (MPa)	Density (kg m^{-3})
Sediment	23–19°	20–50%	1	2800
Subduction interface	5°	–	1	2800
Oceanic crust	50°	–	10	3000

[a] Hydrostatic fluid pressure is assumed. Frictional values for sediment are based on minimum and maximum estimates from Kukowski (2004). The sediment has a small, initial random variation in frictional strength (±1°).

The criterion for significant weakening of sediment that we use here, is that weakening occurs when effective pressure becomes negative, so that fluid pressures exceed lithostatic pressure, i.e.,

$$p_{eff} < 0 \quad (1)$$

where

$$p_{eff} = P_{f0} + \rho_s(1-\phi)gz + \rho_w\phi S_w gz + \rho_h\phi S_h gz + \rho_g\phi S_g gz - P_f. \quad (2)$$

P_{f0} is the fluid pressure at the seafloor; P_f is the fluid pressure at depth z where effective pressure is being calculated; g is gravity, ρ_s, ρ_w, ρ_h, and ρ_g, are densities of sediment, water, hydrate and gas respectively, S_w, S_h and S_g are relative saturations of water, hydrates and gas; and ϕ is porosity. This criterion is in most cases too stringent, as the sediment is likely to yield first at lower fluid pressures, either by shear failure (when deviatoric stress is sufficiently high to overcome yield) or by tensile failure (where fluid pressure exceeds minimum compressive stress). However, since we do not know *a priori* the stress state of the sediments, we use the negative effective pressure criterion as an absolute limit. It should be noted, however, that Eq. (2) also neglects cohesive strength. Gas hydrate can also considerably increase the shear strength of sediment (e.g., Winters et al., 2004; Yun et al., 2005; Sultan, 2007; Yun et al., 2007; Winters et al., 2007). Sultan (2007) found empirically that angles of friction increased from ca. 32° to 48° approximately linearly as gas hydrate volume increased to 7%. However, these friction angles are extremely high compared to most sediment near the seafloor and probably an overestimate (Kukowski, 2004; Wang and Hu, 2006). Yun et al. (2007) found significant alteration in frictional strength for gas hydrate concentrations >40% of pore space, although Winters et al. (2007) show that this effect is reduced somewhat when free gas is present. Nevertheless, if formation and dissociation of gas hydrate near the seafloor cause a variation in frictional strength, then this will affect the predictions of mechanical weakening made in the following sections. It may also promote seafloor erosion on slope, because a large contrast between strong, cohesive sediments containing hydrates and weaker, overlying (non-hydrate) sediments could act as a plane of weakness for slope failure.

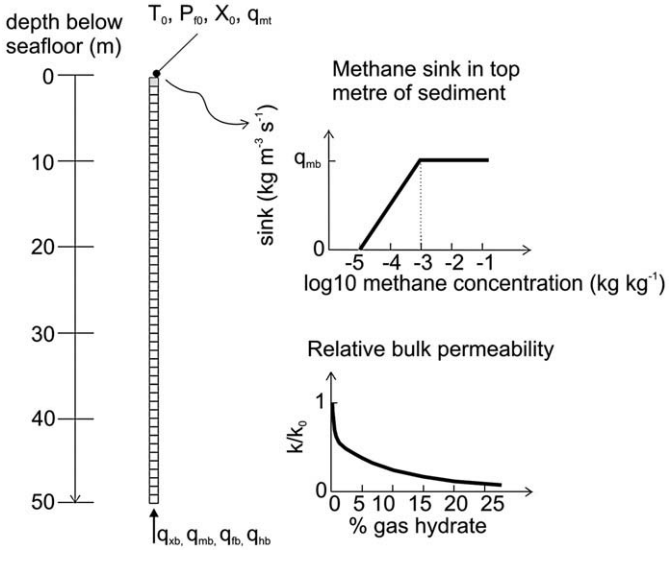

Fig. 5. 1D gas hydrate model setup and initial conditions. Fluxes of salt (q_{xb}), methane (q_{mb}), fluid (q_{fb}) and heat (q_{hb}) are specified at the base of the model. At the seafloor, temperature (T_0), pressure (P_{f0}), salt concentration (X_0) and methane flux (q_{mt}) are specified. A sink term with a maximum value equal to q_{mb}, is applied in the top metre as shown in the inset at top right. All other parameter values are listed in Table 2. Inset at lower right shows the change in relative bulk permeability with increasing hydrate concentration.

4.1. One-dimensional gas hydrate model — setup and steady-state solution

The 1D gas hydrate model assumes a constant sediment density and thermal diffusivity with depth, and a latent heat source term representing the formation and dissociation of gas hydrate. Gas composition is assumed to be 100% methane. Fluid, heat, and methane fluxes are specified at the base of the model, while temperature, pressure, salt concentration and methane flux are specified at the top of the model (Table 2). Heat-flow boundary conditions are based on BSR observations along the subduction margin, which predict a corrected basal heat-flow value of ca. 45 mW/m^2 (Townend, 1997; Henrys et al., 2003b).

Because the process of gas-hydrate-related seafloor weakening is thought to occur over large areas in order to cause flattening of the ridges, we aim to investigate the behaviour of a gas hydrate system away from small-scale features such as gas chimneys. Hence, we make no attempt to model the transport of gas via an upwardly propagating gas chimney (Wood et al., 2002; Liu and Flemings, 2006, 2007).

4.1.1. Top methane boundary condition

Methane concentration can decrease near the seafloor because of anaerobic oxidation of methane (AOM) owing to activity from bacteria and other chemical reactions (e.g., Borowski et al., 1996, 1999). The extent of this zone can be approximated by the depth beneath the seafloor where all methane has been consumed (the depth to the sulphate–methane interface, Z_{SMI}). Within active seeps at Rock Garden, methane is present throughout the sediment column and is released at the seafloor, implying that at some locations the depth Z_{SMI} tends to zero. We have modified the code described by Xu (2004) to account for this observation: Rather than prescribing a zero concentration of methane at the seafloor, we represent the oxidation of methane via sulphate reduction in the top metre of sediment in

Table 2
Initial and material properties for gas hydrate 1D model.

Bulk permeability (m^2)	10^{-16} (high flux case)[a]
	10^{-18} (low flux case)[a]
Porosity (%)	56
Hydrate composition	100% methane
Basal heat flow (mW m^{-2})	45
Basal salt flux (kg m^{-2}s^{-1})	3.2×10^{-9} (high flux case)
	3.2×10^{-11} (low flux case)
Basal methane flux (kg m^{-2}s^{-1})	1.17×10^{-10} (high flux case)
	1.17×10^{-12} (low flux case)
Basal fluid flow (kg m^{-2}s^{-1})	1×10^{-7} (high flux case)
	1×10^{-9} (low flux case)
Uplift rate (mm yr^{-1})	0 or 5
Sink methane term in top m of sediment (kg m^{-3}s^{-1}),	1.17×10^{-10}
Lower–upper thresholds (kg kg^{-1})	(0–1.08×10^{-3})
Sediment density (kg m^{-3})	2650
Thermal conductivity (W m^{-1}K^{-1})	1.174
Enthalpy of hydrate dissociation (kJ kg^{-1})	430

[a] Modified by relative permeabilities for liquid and gas, as described in text.

Please cite this article as: Ellis, S., et al., Testing proposed mechanisms for seafloor weakening at the top of gas hydrate stability on an uplifted submarine ridge (Rock Garden), New Zealand, Marine Geology (2009), doi:10.1016/j.margeo.2009.10.008

terms of a finite sink. The strength of the sink term is proportional to the local methane concentration up to a limiting value (here prescribed as $1.08\times10^{-3}\,\mathrm{kg\,m^{-3}\,s^{-1}}$) above which methane flux overwhelms AOM so that methane is present to the seafloor (Fig. 5). This allows a dynamic boundary where considerable methane concentrations can build up close to the seafloor, providing there is a sufficient flux of methane from below. By varying the methane flux, q_{mb}, entering the base of the 1D model, we can therefore simulate the effects of seep vs. non-seep sites (Tables 2 and 3). Although our method is relatively simple compared to the technique employed in other models such as Davie and Buffett (2003), we will show in Section 4.2 that it is sufficient to reproduce to first-order the observed presence of seep sites, where methane reaches the seafloor, at Rock Garden. However, the models do not investigate short-term variations in methane fluxes as described in Linke et al. (2009 — this issue).

4.1.2. Dependence of bulk permeability on hydrate concentration in the model

We use a permeability model based on the assumption that hydrate forms in the centre of capillary tubes, where bulk permeability depends on hydrate concentration and relative liquid and gas permeabilities are a function of effective saturations (Kleinberg et al., 2003; Liu and Flemings, 2007, as outlined in their equations (21), (25–26) and shown in their Fig. 3). A substantial decrease in bulk permeability of the sediment is predicted as a function of reduced porosity owing to increasing hydrate content, as shown in Fig. 5.

4.2. Results — no temperature or pressure variations

Fig. 6A shows the predicted depth to the bottom of the gas hydrate stability zone (BGHSZ) when hydrate build-up is not limited by methane flux from below, and assuming a bottom-water temperature of 8 °C at 600 m water depth, decreasing at 0.4 °C/100 m extra water depth (Faure et al., 2009 — this issue). This figure predicts that the gas hydrate zone should pinch out at a bottom-water depth of ca. 630 m, close to the depth predicted in Pecher et al. (2005, 2008), and corresponding to the depth at which BSR pinch-outs are observed at Rock Garden.

For 1D modelling taking into account reasonable flux of methane and fluids from below, Fig. 6B–C illustrates the resulting hydrate percent saturation for two water depths. Models M1-640 and M1-680 (Tables 2 and 3) have fluid fluxes and initial bulk permeability representing conditions near methane seeps and zones of elevated fluid flow (e.g., Mann and Kukowski, 1999), at water depths of 640 m and 680 m, respectively. For Model M1-640, the predicted base of the theoretical gas hydrate stability field is only a few metres below the seafloor (Fig. 6A). After ca. 200 kyr, sufficient concentrations of methane have built up to form a maximum concentration of 10% gas hydrate at these shallow depths (Fig. 6B). In contrast, Model M1-680 has a water depth of 680 m, and the predicted depth to the base of the theoretical gas hydrate stability field is 35 m. This model takes longer (700 kyr) to build up a maximum of 10% hydrate in the pore spaces, but the gas hydrate occurs over a greater thickness (Fig. 6C). However, owing to the flux conditions imposed here, the actual gas hydrate zone is thinner than that predicted from the theoretical stability limits (e.g., Xu and Ruppel, 1999).

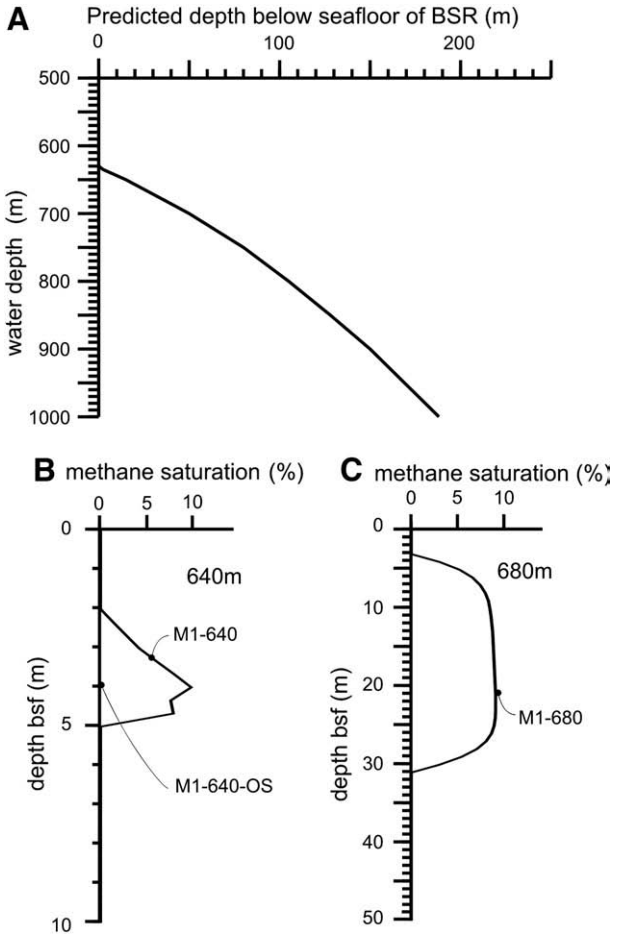

Fig. 6. (A) Theoretical depth to the bottom of the gas hydrate stability zone applying depth-dependent hydrostatic fluid pressure above the seafloor, a bottom-water temperature variation with depth based on Faure et al. (2009 — this issue), and assuming an unlimited methane flux from below. The BSR is predicted to outcrop at the seafloor at a depth of ca. 630 m bsl. (B) Predicted hydrate saturation after 212 kyr for 1D gas hydrate model and seafloor depth of 640 m, starting from an initial methane concentration of $10^{-4}\,\mathrm{kg\,kg^{-1}}$. Parameter values from Tables 2 and 3. Model M1-640 has about 10% hydrate in upper few metres. Model M1-640-OS (with lower bottom methane flux, Table 2) does not form hydrate. (C) Model M1-680, predicted hydrate saturation after 675 kyr for 1D gas hydrate model and seafloor depth of 680 m. Note that the plots shown in Fig. 6B-C were constructed assuming a constant seafloor temperature of 8 °C, since the decrease in temperature with depth is relatively minor. Other parameter values are listed in Tables 2 and 3.

An additional model (M1-640-OS) was run representing off-seep (OS) conditions at 640 m water depth, with lower background permeability and lower fluid and methane flux rates from below (Table 2). No methane hydrate accumulated in this model before it reached a steady state. The low fluxes from below were easily absorbed by the surface sink in methane (representing the zone where methane is oxidised), so that little methane was present in the top 10 m of sediment.

Table 3
List of 1D gas hydrate models.

Model number	Seafloor temperature (°C)	Seafloor pressure (MPa)	Salient details
M1-640	8	6.4	High flux case, 640 m water depth, run until 10% hydrate
M1-640-OS	8	6.4	Low flux case (did not generate hydrate)
M1-680	8	6.8	High flux case, 680 m water depth, run until 10% hydrate
M2-10 yrs	8 ± 1	6.4	Starts from M1-640, 10 year cyclic temperature periodicity at seafloor
M2-100 yrs	8 ± 1	6.4	Starts from M1-640, 100 year cyclic temperature periodicity at seafloor
M3-UP	8	6.8–6.05	Starts from M1-680, uplifts at 5 mm/yr

Please cite this article as: Ellis, S., et al., Testing proposed mechanisms for seafloor weakening at the top of gas hydrate stability on an uplifted submarine ridge (Rock Garden), New Zealand, Marine Geology (2009), doi:10.1016/j.margeo.2009.10.008

4.3. Results — cyclical temperature variations on a timescale of 10–100 years

Cyclical temperature changes were imposed at the seafloor to the steady-state models described above, in order to test Hypothesis 2a — that repeated formation and dissociation of gas hydrates near the seafloor, caused by variations in bottom-water temperature, are sufficient to cause pressure fluctuations that destabilise sediment. We based the amplitude and periodicity of bottom-water temperature fluctuations on the CTD probe results as discussed by Pecher et al. (2008). These suggest a temperature variation of at least ±1 °C, over timescales much greater than the 160-day cycle suggested in 2005 (Pecher et al., 2005, 2008; Faure et al., 2009 — this issue). To simplify, we test the effect of temperature cycles varying over intervals of 10 and 100 years.

Initial conditions for models M2-10 yrs and M2-100 yrs (Table 3) are based on the high flux case with 640 m water depth, starting from Model M1-640 (Fig. 6B). That is, we assume that prior to the onset of the thermal fluctuation a small amount of gas hydrate (10%) has formed just above the theoretical base of the gas hydrate stability zone. A sinusoidal variation in seafloor temperature of ±1 °C is then imposed, with a period of 10 years (Fig. 7A–D) or 100 years (Fig. 7E–H). The temperature fluctuations penetrate the seafloor with an amplitude that diminishes with depth, and shifts in phase, depending on thermal parameters and the effect of the hydrate already present (e.g., Sultan et al., 2004; Pecher et al., 2005). Penetration for the 100–year fluctuation is deeper compared with the 10-year fluctuation (Fig. 7A, E). A slight evolution in the temperature field with time is also observed in both cases, which we attribute to the effect of latent heat during the formation and dissociation of gas hydrate.

Model M2-10 yrs shows a gradual evolution in the location of hydrate in the uppermost 10 m of the model. The hydrate dissociates during each upward swing in temperature, and re-forms during the following down-swing at a slightly shallower level (Fig. 7B). In contrast, Model M2-100 yrs, with a longer period over which the temperature fluctuation occurs, shows a sudden jump in the depth of hydrate between the first and second cycles, with fairly steady behaviour thereafter (although a slight oscillation develops in the solution, which is evident from the granularity for times >400 years) (Fig. 7F).

Analysis of the effective pressure for both models illustrates the effect on gas hydrate occurrence (Fig. 7C, G). Effective pressure reduces (i.e., fluid pressure increases) during gas hydrate formation at shallow levels — with a much lesser effect in the initial stages of each model, when hydrate is located at depths >3 m. We emphasize that the reduction in effective pressure — i.e., the increase in fluid pressure — occurs during gas hydrate association, not dissociation and is thus not caused by volume expansion from a release of gas. We think that the increase in fluid pressure accompanying hydrate growth is caused by the reduction in permeability as hydrate fills the pore space, constricting fluid flow. This effect is much more pronounced for the case with 100-year periodicity, not because the thermal pulse penetrates deeper, but because hydrate formation is enhanced in the top 2 m. As a result, fluid pressure actually exceeds lithostatic pressure in the top 2 m for a part of the second cycle (Fig. 7G; white area indicates negative effective pressure). A plot of the effective pressure profile with depth at this time (Fig. 7H) illustrates this, although it is clear that the reduction in effective pressure is relatively minor. The negative effective pressure is not repeated in subsequent cycles, because the amount of hydrate in the top 2 m of sediment diminishes as methane concentration reduces owing to the flux through the top boundary.

In both models, the initial presence of hydrate at depth is critical for the strong effect of gas hydrate formation on pressure. Further tests have shown that without this initial layer, methane concentrations are insufficient to generate significant amounts of hydrate at shallow depths during temperature down-swings.

Although the effect on pressure shown in Fig. 7G–H is interesting, the fluctuation in effective pressure is very small and short-lived. We show in the following section that a larger and more prolonged effect on effective pressure can result from uplift of hydrate-bearing layers through the gas hydrate stability limit.

4.4. Results — transient models: effect of ridge uplift on hydrate stability

When material uplifts above a subducting seamount (e.g., Section 3), there will be a significant change in the hydrostatic pressure acting at the seafloor, creating a change in the conditions for gas hydrate stability and possibly leading to fluid pressure changes owing to the change in state from solid gas hydrate to water and free/dissolved gas (Hypothesis 2b; Xu and Ruppel, 1999; Xu and Germanovich, 2006).

To test this hypothesis, in Model M3-UP we imposed a linear decrease in the top pressure boundary condition of the 1D models. We did not model the entire uplift history of the ridge, but instead tested the effect of the last 75 m of uplift starting from the end point of Model M1-680 (i.e., the seep case starting at a water depth of 680 m with a maximum hydrate content of 10%) (Table 3). Pressure at the top boundary was linearly decreased from 6.8 MPa to 6.05 MPa over 15 kyr, corresponding to an uplift rate of 5 mm/yr (i.e. somewhat lower than maximum uplift rates derived from the mechanical modelling in Section 3; Fig. 4), where it is assumed that no erosion is occurring. The bottom-water temperature was kept constant at 8 °C.

Fig. 8A shows the evolution in gas hydrate content as a function of time since the onset of uplift. As in previous models (e.g., Xu and Germanovich, 2006) the seafloor pressure change causes dissociation of gas hydrate at the base of the stability zone, after a time lag of about 5 kyr (Fig. 8A, C). Once dissociation begins, owing to the increase in permeability when the hydrate dissociates, some of the methane released in this zone re-forms at the new base of the hydrate stability zone, causing an increase in the hydrate content there (Fig. 8C). Gas hydrate lingers into sediment depths of 5 m even when the water depth decreases to almost 600 m, i.e. above the theoretical limit calculated in Fig. 6A. This is because of the time lag between instantaneous changes in ambient pressure and temperature conditions and the melting of hydrate.

Fig. 8B plots the effective pressure for Model M3-UP. As for the models discussed in Section 4.3, the greatest pressure increase is observed at shallow depths once gas hydrate begins to form there — within, not beneath, the gas hydrate-bearing zone. We think that this is caused by the strong dependence of permeability on hydrate content used in our models (cf. Xu and Germanovich (2006)). For a hydrate content of 10%, the relative permeability of fluid is reduced to 30% of its value when no hydrate is present (Liu and Flemings, 2007). The reduction in permeability prevents the escape of methane and fluid, while hydrate claims a greater proportion of available pore space, raising ambient fluid pressures. The pulse of increased fluid pressure moves upward in time (along with the peak in hydrate concentration; Fig. 8B and C). As this pressure pulse moves upward, it becomes a great fraction of total (overburden) pressure, until at ca. 625 m water depth, fluid pressures exceed lithostatic pressure, causing negative effective pressure. Before this occurs, the sediment is likely to lose all mechanical strength, either by shear or tensile failure (as discussed at the start of Section 4).

This model result suggests that Hypothesis 2b may be an effective way to weaken sediment as a result of the change in hydrate saturation caused by tectonic uplift. The effect is only significant when the hydrate layer approaches the seafloor, thus providing a possible explanation for the coincidence in BSR pinch-out and flattening slopes.

5. Discussion

5.1. Effect of seafloor temperature fluctuations

The models testing Hypothesis 2a (sediment weakening due to thermal cycling at the seafloor) show how temperature perturbations

Please cite this article as: Ellis, S., et al., Testing proposed mechanisms for seafloor weakening at the top of gas hydrate stability on an uplifted submarine ridge (Rock Garden), New Zealand, Marine Geology (2009), doi:10.1016/j.margeo.2009.10.008

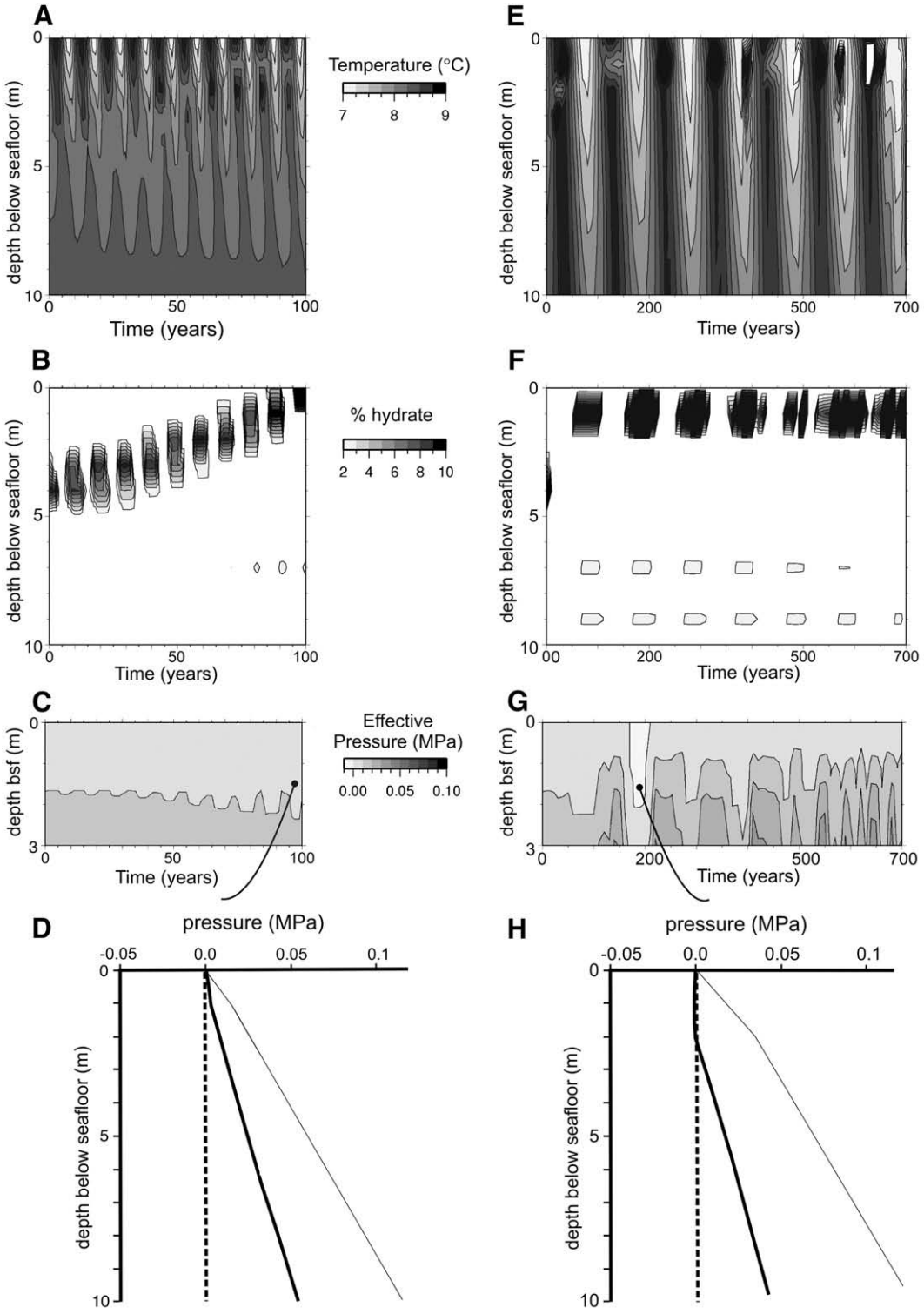

Fig. 7. (A–D) Model M2-10 yrs — result of a cyclical change in bottom-water temperature of ± 1 °C over 10 years, on (A) temperature beneath the seafloor; (B) % hydrate saturation; and (C) effective pressure as defined in Eq. (2) in the text. Model M2-10 yrs began from the end state of Model M1-640 of Fig. 6(B). (D) Profile of effective pressure (bold solid line) and total fluid pressure minus seafloor pressure (thin solid line) after 10 cycles. (E–H) Model M2-100 yrs — result of a cyclical temperature change of ± 1 °C over 100 years, showing (E) temperature, (F) % hydrate saturation, and (G) effective pressure. (H) Profile of effective pressure (bold solid line) and total fluid pressure minus seafloor pressure (thin solid line) after 2 cycles.

can cause periodic formation and dissociation of gas hydrates when a high flux of methane can be generated by dissociation of deeper hydrate layers. Similarly, Sultan et al. (2004) investigated the effect of a 230-day-period temperature variation on gas hydrate distribution near the surface for the Congo continental slope. They found that the transient thermal signal penetrated ca. 2 m in saturated sediment and around 6 m in hydrate-bearing sediments, but that the switch from gas hydrate to gas and back only occurred in the top metre of their 1D model. With the longer time variations investigated here, penetration of the thermal perturbation was deeper, but the effect on the effective strength of sediment was shown to be small and limited in time (Section 4.3). Our models therefore suggest that repeated dissociation

Please cite this article as: Ellis, S., et al., Testing proposed mechanisms for seafloor weakening at the top of gas hydrate stability on an uplifted submarine ridge (Rock Garden), New Zealand, Marine Geology (2009), doi:10.1016/j.margeo.2009.10.008

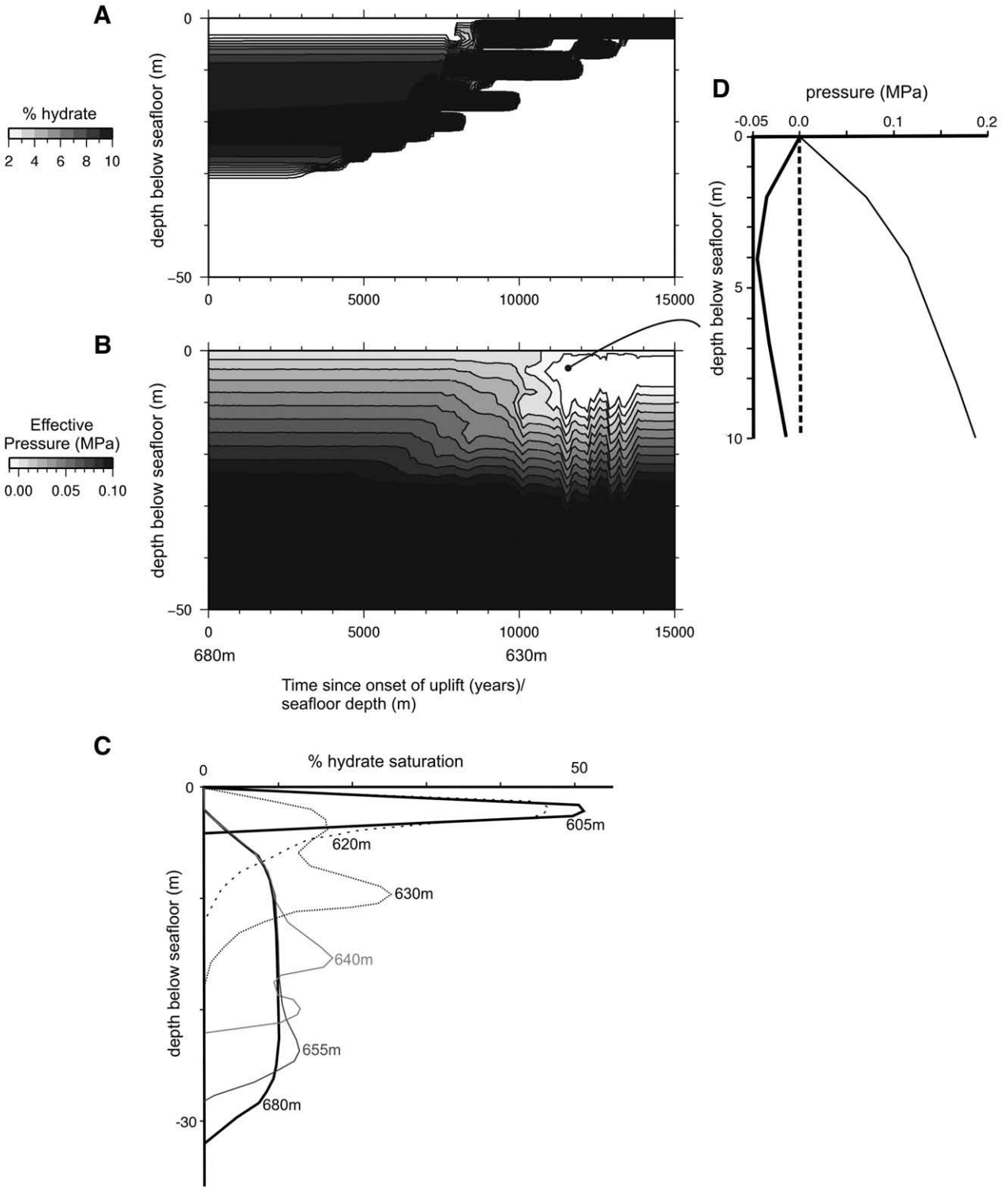

Fig. 8. Model M3-UP, showing effect of tectonic uplift (decreasing water load) on a model that starts from Model M1-680 (at 680 m water depth). Uplift of 5 mm/yr for 15 kyr applied, corresponding to a change in depth to seafloor from 680 m to 605 m. (A) % hydrate saturation. (B) Effective pressure; white indicates areas with negative effective pressure (MPa). (C) Profile showing evolution in hydrate saturation with depth and time, illustrating focusing effect and shallowing caused by uplift. (D) Profile of effective pressure (bold solid line) and total fluid pressure minus seafloor pressure (thin solid line) at 11 kyr, showing negative effective pressures in top 10 m of sediment. Note that the base of the gas hydrate at this time is at a depth of 12 m.

and formation of gas hydrates are unlikely to cause widespread weakening of the seafloor. We also note that the shortest time-scale we present here is 10 years, probably longer than the actual setting and much longer than the originally proposed 100–200 days.

This mechanism may work if there is a stronger dependence of permeability on hydrate content, and a larger initial hydrate "pool" that can be dissociated. For example, if lateral flow of gas occurs along the BSR (e.g., as pointed out by Crutchley et al. (2009 — this issue)), larger bottom fluxes of methane and fluids may be present than investigated here (Table 2). Subsequent hydrate dissociation could then lead to significant excess pore fluid pressure as discussed by Xu and Germanovich (2006).

Please cite this article as: Ellis, S., et al., Testing proposed mechanisms for seafloor weakening at the top of gas hydrate stability on an uplifted submarine ridge (Rock Garden), New Zealand, Marine Geology (2009), doi:10.1016/j.margeo.2009.10.008

Most current models of gas hydrate formation focus on porous media with reasonable porosities and permeabilities. Should mudstone be prevalent beneath Rock Garden, these models may not be appropriate. Mudstones display little primary permeability; however, if fractured, they tend to exhibit significant secondary (or structural) permeability. It is conceivable that capillary forces in consolidated mudstones (Henry et al., 1999; Clennell et al., 1999; Anderson et al., 2003a,b) could lead to fracturing and/or dilation of existing fractures, ultimately decreasing the strength of the seafloor. In this case, the ice-like growth of hydrate crystals during association would push aside the walls of thin fractures. Dissipation of overpressure during gas hydrate dissociation would not affect this process. On the other hand, capillary forces are also linked to hysteresis — in fine-grained sediments, gas hydrate formation may require up to several degrees Celsius cooler temperatures than its dissociation — and both curves lie below the phase boundary in water (Anderson et al., 2003a,b). Significant hysteresis would make repeated dissociation and formation of gas hydrates less likely because large temperature fluctuations would be required. It is particularly tempting to implicate capillary forces during gas hydrate "freeze–thaw" cycles in fracturing of mudstones because repeated freezing is an established laboratory procedure for disaggregating mudstones (Yang and Aplin, 1997). Accordingly, repeated dissociation and formation of gas hydrates can still not be ruled out entirely as an explanation for the flat morphology at Rock Garden however, if they do take place, the process is more complicated than previously thought.

5.2. Effect of tectonic uplift

Hypothesis 2b, mechanical weakening caused by uplift of sediments containing gas hydrates, appears to be a possible way to cause seafloor erosion (Section 4.4; Pecher et al., 2005). Rapid uplift leads to progressive dissociation of gas hydrate at the base of the hydrate stability zone, and formation of hydrate at shallower depths. At some stage, the concentration in hydrate approaching the surface causes a large increase in fluid pressure, leading to low or negative effective pressures, which will facilitate sediment shear or tensile failure. For this mechanism to work, it is critical that bulk permeability is reduced quite strongly during hydrate association of more than a few percent. In order to investigate this effect further, experiments that critically constrain the dependence of gas and liquid permeability on hydrate content are needed, and more observations are required from dredged sediment at the seafloor.

According to Xu and Germanovich (2006), dissociation of hydrate should be accompanied by an increase in fluid pressure owing to the relative expansion of gas. This effect is predicted to be greatest for low-permeability ("closed" systems (Xu and Germanovich, 2006)). In our model runs, we found that this effect was far outweighed by the effect of decreasing permeability during hydrate formation, although it may have become important had we considered systems with much lower sediment permeabilities.

5.3. The effect of bottom currents on sediment erosion

It has been previously shown that bottom currents are able to efficiently erode the seafloor. Clift et al. (2003) quantified very roughly the amount of seafloor erosion in order to subtract the subduction erosion signal. Averaged over millions of years, the seafloor erosion rate was found to be quite high (300 m in 10 My). Weakened (unlithified) sediment is necessary for the rates to become significant. Holbrook et al. (2002) suggested that the Blake Ridge depression in the western Atlantic is a large sediment-wave field, with erosion and deposition rates varying strongly in space and time. At Rock Garden, bottom-water currents may provide the explanation for removal of weakened sediment, where the weakened sediment results from one or several of the processes investigated in Section 4. Unlike Blake Ridge, sedimentation is unlikely to occur in this environment. An alternative weakening method, not investigated here, is that the contrast between hydrate-rich layers and less consolidated surface layers within the sulphate reduction zone may enhance surface erosion by bottom currents; but it is unclear why this contrast would promote erosion at water depths of ~600 m only.

5.4. Sediment failure mechanisms within and beneath hydrate layers

We have used negative effective pressure as a proxy for mechanical failure. In real sediments, failure will occur before this proxy limit is reached, at pressures close to but below lithostatic, as a result of shear or tensile failure. Sediment frictional strength and cohesion are likely to control the maximum effective pressure the sediment supports, and gas hydrates are known to increase sediment cohesion. While Model M3-UP (Figs. 8 and 9) predicts maximum overpressure within the hydrate zone, failure may still occur within weaker hydrate-free sediments beneath this layer, at the BGHS, as it approaches the surface.

Previously, the main concern with implicating hydrate dissociation at the BGHS in seafloor weakening on Rock Garden was the presence of BSR pinch-outs at the ridge crests. BSR pinch-outs are thought to mark the top of gas hydrate stability in the ocean for an average water temperature, although Pecher et al. (2005) note that warm fluids may locally cause the BGHS to approach the seafloor at the edges of the ridge crests, while the ridge summits still remain within the regional gas hydrate zone. The presence of shallow reflections that are interpreted as BSRs beneath parts of the ridge plateau, with pinch-outs beneath vent sites (Crutchley et al., 2009 — this issue), underscores the viability of BSR/ridge intersections as a potential control on sediment weakening.

5.5. The presence of gas hydrate outside of the steady-state stability zone

An interesting aspect of the model shown in Section 4.4 (M3-UP) is that gas hydrate occurs at shallower depths than predictions of the base of the gas hydrate stability zone from theoretical considerations (Fig. 8C vs. Fig. 6A), making it possible that methane gas hydrate is present beneath much of the ridge crest even though the ridge is located above the "static" methane hydrate stability zone. This is a temporal effect and with further uplift (or quiescence) the hydrate layer vanishes. It also illustrates the potential problem in interpreting BSR depth in terms of heat-flow and steady-state conditions, when in an actively uplifting tectonic area.

We caution that the depth and duration of this meta-stable gas hydrate layer are strongly dependent on both input parameters for our modelling and probably, the type of gas hydrate formation model. However, our modelling shows at least qualitatively that it is conceivable to encounter gas hydrates beneath an uplifting seafloor above the top of gas hydrate stability as marked by BSR pinch-outs.

5.6. Other possible causes of overpressure

The effects of elevated salinity caused by hydrate formation have been modelled by Liu and Flemings (2006), who suggest that this can generate three-phase equilibrium, allowing free gas migration to the surface. This process may drive gas venting through hydrate stability zones, and locally cause disruption and weakening of sediment. However, studies from the Blake Ridge (Henry et al., 1999) suggest that the presence of a gas column requires an interconnected gas phase with a volume fraction larger than ~20% of pore space. Usually these are localized phenomena that would be unable to explain the presence of flat ridge morphology over a significant area, but the presence of vent fields up to half a square kilometre large (Greinert et al., this volume) may suggest that gas migration is more than localized near Rock Garden. Numerous gas pockets have been observed near

Please cite this article as: Ellis, S., et al., Testing proposed mechanisms for seafloor weakening at the top of gas hydrate stability on an uplifted submarine ridge (Rock Garden), New Zealand, Marine Geology (2009), doi:10.1016/j.margeo.2009.10.008

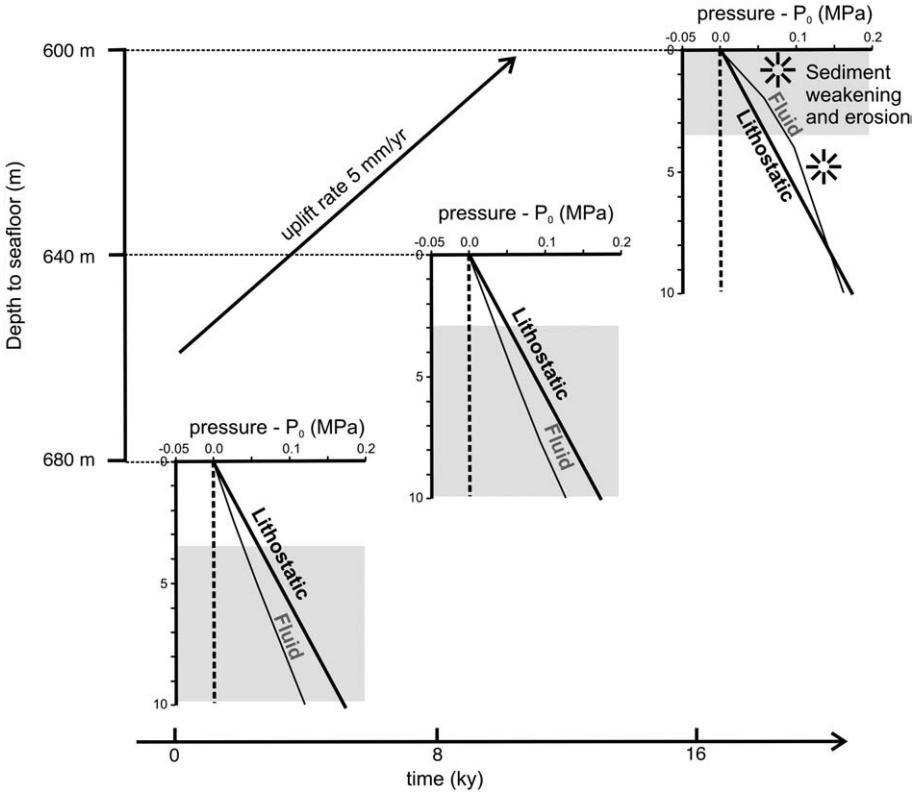

Fig. 9. A cartoon illustrating the preferred mechanism for sediment weakening caused by progressive uplift of a layer containing gas hydrate. Bold line is lithostatic pressure, thin line is fluid pressure, both corrected for seafloor pressure (P_{f0}). Shaded region is gas hydrate. Progression from left to right shows upward migration of hydrate layer, with increasing fluid pressure, until at shallow levels fluid pressure approaches and exceeds lithostatic pressure. As fluid pressure approached lithostatic, shear or tensile failure occurs, causing sediment weakening (burst symbol). Sediment is then eroded by bottom currents and/or internal waves.

the seafloor beneath Rock Garden (Crutchley et al., 2009 — this issue). Conceptual 2D two-phase modelling of fluid and gas pressure beneath a thin gas-hydrate zone, based on seismic images from Rock Garden, shows that gas buoyancy may contribute significantly to overpressure (Crutchley, 2009). As suggested here, Crutchley (2009) postulate that permeability reduction in the gas hydrate stability zone is a key factor controlling overpressure.

5.6. Global implications of this study

Eroded sub-sea ridges with BSR pinch-outs on the edges of flat tops have not been reported from other gas hydrate regions in the world, to our knowledge. One factor that may be unique to our study area is that recently deposited sediments and/or weakened sediments on Rock Garden and Ritchie Banks are mobilized by bottom-water currents and/or slide down the steep flanks of the ridges, making the ridges a non-sedimentary environment. The steep slopes flanking the ridge result from compacted sediments, unlike the soft sediments that host gas hydrates in most other regions. Dredge samples from Rock Garden suggest that the country rock on Rock Garden is consolidated but fractured mudstone (Pecher et al., 2008). Permeability in these rocks may be controlled by fracturing (e.g., Pecher et al., this issue). A decrease of permeability with hydrate saturation is a key to our favoured hypothesis for sediment weakening during tectonic uplift. It is conceivable that clogging of secondary permeability in fractures after hydrate formation is different from primary permeability in porous media. We speculate however, that our proposed mechanisms for sediment weakening may take place elsewhere, but that rather than leading to flat tops of uplifted ridges, these mechanisms may be hidden beneath recent sedimentation.

6. Conclusions

Several hypotheses for the formation of a flat-topped ridge near the intersection depth of the gas hydrate stability zone and the seafloor, offshore North Island, New Zealand have been tested using 2D mechanical and 1D gas hydrate modelling. Preliminary conclusions indicate that:

- Tectonic uplift above a seamount can sometimes cause flat ridge morphology, but this is a transient process. Such an effect may enhance the flat-shaped nature of Rock Garden but is unlikely to be the dominant cause for its morphology.
- The most plausible mechanism for sediment weakening on the ridge was found to be the effect of tectonic uplift on gas hydrates, focusing methane fluxes and causing a cumulative increase in hydrate saturation that approaches the seafloor, lowering permeability there and enhancing fluid pressure until fluid pressures are sufficiently high to cause shear or tensile failure in the sediments (Fig. 9).
- 1D modelling suggests that tectonic uplift can lead to transient layers of gas hydrate at shallower depths than predicted for steady-state theoretical considerations, so that methane gas hydrate may be present beneath much of the ridge crest even though the ridge is located above the “static” methane hydrate stability zone.
- Fluctuations in bottom-water temperature are capable of inducing periodic hydrate formation/dissociation, especially when methane concentrations are enhanced by dissociation of underlying hydrate layers. However, for the hydrate concentrations investigated here, the effect on fluid pressures is not as great as for the tectonic uplift mechanism.
- The preferred mechanism, fluid overpressure leading to sediment weakening during hydrate formation, depends critically on the

Please cite this article as: Ellis, S., et al., Testing proposed mechanisms for seafloor weakening at the top of gas hydrate stability on an uplifted submarine ridge (Rock Garden), New Zealand, Marine Geology (2009), doi:10.1016/j.margeo.2009.10.008

assumed decrease in permeability with increasing hydrate saturation. Further empirical work is needed on the relationship between permeability and hydrate to fully constrain this effect.

Acknowledgements

Funding for this study was provided by a Royal Society of New Zealand Marsden Grant, contract number GNS0403, and Foundation for Research Science and Technology Contract C05X0703. Jens Greinert thanks the European Union for financial support and the possibility to work at GNS Science and RCMG via a Marie Curie grant (MOIF-CT-2005-007436). We thank Gareth Crutchley and two anonymous reviewers for their constructive comments on the manuscript, and Steve Chiswell for advice on ocean currents at Rock Garden. The mechanical code was developed jointly with Susanne Buiter from NGU, Norway. Some of the figures were plotted using GMT (Generic Mapping Tools) software.

References

Anderson, R., Llamedo, M., Tohidi, B., Burgass, R.W., 2003a. Characteristics of clathrate hydrate equilibria in mesopores and interpretation of experimental data. Journal of Physical Chemistry. B 107, 3500–3506.

Anderson, R., Llamedo, M., Tohidi, B., Burgass, R.W., 2003b. Experimental measurement of methane and carbon dioxide clathrate eydrate equilibria in mesoporous silica. Journal of Physical Chemistry. B 107, 3507–3514.

Barnes, P., Mercier de Lépinay, 1997. Rates and mechanics of rapid frontal accretion along the very obliquely convergent southern Hikurangi Margin, New Zealand. Journal of Geophysical Research 102 (B11), 24931–24952.

Barnes, P.M., Lamarche, G., Bialas, J., Henrys, S., Pecher, I., Netzeband, G., Greinert, J., Mountjoy, J.J., Pedley, K., and Crutchley, G.J., 2009-this issue. Tectonic and geological framework for gas hydrates and cold seeps on the Hikurangi Subduction Margin, New Zealand. Marine Geology.

Borowski, W.S., 2004. A review of methane and gas hydrates in the dynamic, stratified system of the Blake Ridge region, offshore southeastern North America. Chemical Geology 205, 311–346.

Borowski, W.S., Paull, C.K., Ussler III, W., 1996. Marine pore-water sulfate profiles indicate in situ methane flux from underlying gas hydrate. Geology 24, 655–658.

Borowski, W.S., Paull, C.K., Ussler III, W., 1999. Global and local variations of interstitial sulfate gradients in deep-water, continental margin sediments: sensitivity to underlying methane and gas hydrates. Marine Geology 159, 131–154.

Cacchione, D.A., Pratson, L.F., Ogston, A.S., 2002. The shaping of continental slopes by internal tides. Science 296, 724–727. doi:10.1126/science.1069803.

Clennell, M.B., Hovland, M., Booth, J.S., Henry, P., Winters, W.J., 1999. Formation of natural gas hydrates in marine sediments. Part I: conceptual model of gas hydrate growth conditioned by host sediment properties. Journal of Geophysical Research B10, 22985–23003.

Clift, P.D., Pecher, I., Kukowski, N., Hampel, A., 2003. Tectonic erosion of the Peruvian forearc, Lima Basin, by subduction and Nazca Ridge collision. Tectonics 22, 1023. doi:10.1029/2002TC001386.

Collot, J.-Y., Lewis, K.B., Lamarche, G., Lallemand, S.E., 2001. The giant Ruatoria debris avalanche on the northern Hikurangi Margin, New Zealand: results of oblique seamount subduction. Journal of Geophysical Research 106, 19271–19297.

Crutchley, G.J., Pecher, I.A., Gorman, A.R., Henrys, S.A. and Greinert, J., 2009 — this issue. Seismic imaging of gas conduits beneath seafloor vent sites in a shallow marine gas hydrate province, Hikurangi Margin, New Zealand. Marine Geology.

Crutchley, G., 2009. Gas hydrates on New Zealand's Hikurangi Margin: the importance of focused fluid flow for highly-concentrated deposits, methane seepage, and seafloor erosion, PhD thesis, University of Otago, Dunedin.

Davey, F., Hampton, M.A., Childs, J.R., Fisher, M.A., Lewis, K., Pettinga, J.R., 1986. Structure of a growing accretionary prism, Hikurangi Margin, New Zealand. Geology 14 (8), 663–666.

Davie, M.K., Buffett, B.A., 2003. A steady state model for marine hydrate formation: constraints on methane supply from pore water sulfate profiles. Journal of Geophysical Research 108 (B10), 2495. doi:10.1029/2002JB002300.

Dominguez, S., Lallemand, S.E., Malavieille, J., von Huene, R., 1998. Upper plate deformation associated with seamount subduction. Tectonophysics 293, 207–224.

Dominguez, S., Malavieille, J., Lallemand, S.E., 2000. Deformation of accretionary wedges in response to seamount subduction: insights from sandbox experiments. Tectonics 19, 182–196.

Faure, K., Greinert, J., 2006. Methane Seepage and its relation to slumping and gas hydrate at the Hikurangi Margin, New Zealand. New Zealand Journal of Geology and Geophysics 49, 503–516.

Faure, K., Greinert, J., Schneider von Deimling, J., McGinnis, D.F., Kipfer, R., and Linke, P., 2009 — this issue. Free and dissolved methane in the water column and the sea surface: Geochemical and hydroacoustic evidence of bubble transport, Marine Geology.

Fullsack, P., 1995. An arbitrary Lagrangian–Eulerian formulation for creeping flows and its application in tectonic models. Geophysical Journal International 120, 1–23.

Henry, P., Thomas, M., Clennell, M.B., 1999. Formation of natural gas hydrates in marine sediments. Part 2: thermodynamic calculations of stability conditions in porous media. Journal of Geophysical Research 104, 23005–23022.

Henrys, S.A., Ellis, S., Uruski, C., 2003a. Conductive heat-flow variations from bottom-simulating reflectors on the Hikurangi Margin, New Zealand. Geophysical Research Letters 30, 1065–1068. doi:10.1029/2002GL015772.

Henrys, S.A., Reyners, M., Bibby, H., 2003b. Exploring the plate boundary structure of North Island, New Zealand. Eos Transaction, American Geophysical Union 84 (31), 289.

Henrys, S.A., Reyners, M.E., Pecher, I.A., Bannister, S.C., Nishimura, Y., Maslen, G., 2006. Kinking of the subducting slab by escalator normal faulting beneath the North Island of New Zealand. Geology 34, 777–780. doi:10.1130/G22594.1.

Holbrook, W.S., Lizarralde, D., Pecher, I.A., Gorman, A.R., Hackwith, K.L., Hornbach, M., Saffer, D., 2002. Escape of methane gas through sediment waves in a large methane hydrate province. Geology 30, 467–470.

Kleinberg, R.L., Flaum, C., Griffin, D.D., Brewer, P.G., Malby, G.E., Peltzer, E.T., Yesinowski, J.P., 2003. Deep sea NMR: Methane hydrate growth habit in porous media and its relationship to hydraulic permeability, deposit accumulation, and submarine slope stability. Journal of Geophysical Research 108, 2508. doi:10.1029/2003JB002389.

Kobayashi, K., Nakanishi, M., Tamaki, K., Ogawa, Y., 1998. Outer slope faulting associated with the western Kuril and Japan trenches. Geophysical Journal International 134, 356–372.

Kukowski, N., 2004. Material and fluid flux at convergent margins: what ends up in the forearc? In: Bertott, G., Buiter, S, Ruffo, P., Schreurs, G. (Eds.), From Mountains to Sedimentary Basins: Modelling and testing geological processes, Bollettino di Geofisica Teorica ed Applicata, extended abstracts from GeoMod2004 International Conference, Emmetten, Switzerland, pp. 104–108.

Lallemand, S.E., von Huene, R., Culotta, R., 1989. Subduction of the Daiichi Kashima seamount in the Japan trench. Tectonophys 160, 231–247.

Lewis, K.B., Lallemand, S.E., Carter, L., 2004. Collapse in a quaternary shelf basin off East Cape, New Zealand: evidence for passage of a subducted seamount inboard of the Ruatoria giant avalanche. New Zealand Journal of Geology and Geophysics 47, 415–429.

Linke, P., Sommer, S., Rovelli, L., McGinnis, D.F., 2009 — this issue. Physical limitations of dissolved methane fluxes: The role of bottom layer processes, Marine Geology.

Liu, X., Flemings, P., 2006. Passing gas through the hydrate stability zone at southern Hydrate Ridge, offshore Oregon. Earth and Planetary Science Letters 241, 211–226.

Liu, X., Flemings, P., 2007. Dynamic multiphase flow model of hydrate formation in marine sediments. Journal of Geophysical Research 112, B03101. doi:10.1029/2005JB004227.

Mann, P., Kukowski, N., 1999. Numerical modelling of focussed fluid flow in the Cascadia accretionary wedge. Journal of Geodynamics 27, 359–372.

Mienert, J., Posewang, J., Baumann, M., 1998. Gas hydrates along the northeastern Atlantic Margin: possible hydrate-bound margin instabilities and possible release of methane. In: Henriet, J.P., Mienert, J. (Eds.), Gas hydrates; relevance to world margin stability and climatic change: Geol. Soc. Spec. Publ. , pp. 275–291.

Mienert, J., Vanneste, M., Bünz, S., Andreassen, K., Haflidason, H., Sejrup, H.P., 2005. Ocean warming and gas hydrate stability on the mid-Norwegian margin at the Storegga Slide. Marine and Petroleum Geology 22, 233–244.

Moresi, L., Dufour, F., Muhlhaus, H.B., 2003. A Lagrangian integration point finite element method for large deformation modelling of viscoelastic geomaterials. Journal of Computational Physics 184, 476–497.

Naudts, L., Greinert, J., Poort, J., Belza, J., Vangampelaere, E., Boone, D., Linke, P., Henriet, J.P., De Batist, M., this issue. Active venting seep sites on the gas-hydrate-bearing Hikurangi Margin, Off New Zealand: visual observations and measurements. Marine Geology. doi:10.1016/j.margeo.2009.08.002.

Park, J.O., Tsuru, T., Kaneda, Y., Kono, Y., Kodaira, S., Takahashi, N., Kinoshita, H., 1999. A Subducting Seamount beneath the Nankai Accretionary Prism off Shikoku, Southwestern Japan. Geophysical Research Letters 26, 931–934.

Pecher, I.A., Henrys, S.A., Ellis, S., Chiswell, S.M., Kukowski, N., 2005. Erosion of the seafloor at the top of the gas hydrate stability zone on the Hikurangi Margin, New Zealand. Geophysical Research Letters 32, L24603.

Pecher, I.A., Coffin, R., Henrys, S.A., CHARMNZ Working Group, 2007. Cruise Report: Gas Hydrate Exploration on the East Coast, North Island, New Zealand. GNS Science, Lower Hutt, New Zealand. Science Report 2007/29.

Pecher, I.A., Henrys, S.A., Ellis, S., Crutchley, G., Fohrmann, M., Gorman, A., Greinert, J., Chiswell, S.M., 2008. Erosion of seafloor ridges at the top of the gas hydrate stability zone, Hikurangi Margin, New Zealand — new insights from research cruises between 2005 and 2007. Proceedings of the 6th International Conference on Gas Hydrates (ICGH 2008), Vancouver, BC, Canada, July 6–10, 2008. 12 pp.

Pecher, I.A., Henrys, S.A., Wood, W.T., Kukowski, N., Crutchley, G.J., Fohrmann, M., Kilner, J., Senger, K., Gorman, A., Coffin, R.B., Greinert, J., Faure, K., this issue. Focussed Fluid Flow on the Hikurangi Margin, New Zealand: Evidence from Possible Local Upwarping of the Base of Gas Hydrate Stability. Marine Geology.

Rempel, A.W., Buffett, B.A., 1997. Formation and accumulation of gas hydrate in porous media. Journal of Geophysical Research 102, 10151–10164.

Sloan, E.D., 1998. Clathrate Hydrates of Natural Gases. Marcel Dekker, Inc, New York, NY. 705 pp.

Smith, I., Griffiths, D., 2004. Programming the finite element method: with application to geomechanics. John Wiley and Sons. 646 pp.

Sultan, N., 2007. Comment on "Excess pore pressure resulting from methane hydrate dissociation in marine sediments: a theoretical approach" by Wenyue Xu and Leonid N. Germanovich. Journal of Geophysical Research 112, B02103. doi:10.1029/2006JB004527.

Sultan, N., Foucher, J.P., Cochonat, P., Tonnerre, T., Bourillet, J.F., Ondreas, H., Cauquil, E., Grauls, D., 2004. Dynamics of gas hydrate: case of the Congo continental slope. Marine Geology 206, 1–18.

Please cite this article as: Ellis, S., et al., Testing proposed mechanisms for seafloor weakening at the top of gas hydrate stability on an uplifted submarine ridge (Rock Garden), New Zealand, Marine Geology (2009), doi:10.1016/j.margeo.2009.10.008

Townend, J., 1997. Estimates of conductive heat flow through bottom-simulating reflectors on the Hikurangi and southwest Fiordland continental margins, New Zealand. Marine Geology 141, 209–220.

von Huene, R., Reston, T., Kukowski, N., Dehghani, G.A., Weinrebe, W., IMERSE Working Group, 1997. A subducting seamount beneath the Merditerranean Ridge. Tectonophys 271, 249–261.

Wang, K., Hu, Y., 2006. Accretionary prisms in subduction earthquake cycles: the theory of dynamic Coulomb wedge. Journal of Geophysical Research 111, B06410. doi:10.1029/2005JB004094.

Winters, W.J., Pecher, I.A., Waite, W.F., Mason, D.H., 2004. Physical properties and rock physics models of sediment containing natural and laboratory-formed methane gas hydrate. American Mineralogist 89, 1221–1227.

Winters, W.J., Waite, W.F., Mason, D.H., Gilbert, L.Y., Pecher, I.A., 2007. Methane gas hydrate effect on sediment acoustic and strength properties. Journal of Petroleum Science & Engineering 56 (1–3), 127–135.

Wood, W.T., Gettrust, J.F., Chapman, N.R., Spence, G.D., Hyndman, R.D., 2002. Decreased stability of methane hydrates in marine sediments owing to phase-boundary roughness. Nature 420, 656–660. doi:10.1038/nature01263.

Xu, W., 2004. Modeling dynamic marine gas hydrate systems. American Mineralogist 89, 1271–1279.

Xu, W., Germanovich, L.N., 2006. Excess pore pressure resulting from methane hydrate dissociation in marine sediments: a theoretical approach. Journal of Geophysical Research 111, B01104. doi:10.1029/2004JB003600.

Xu, W., Ruppel, C., 1999. Predicting the occurrence, distribution, and evolution of methane gas hydrate in porous marine sediments. Journal of Geophysical Research 104 (B3), 5081–5095.

Yang, Y., Aplin, A.C., 1997. A method for the disaggregation of mudstones. Sedimentology 44, 559–562.

Yun, T.S., Francisca, F.M., Santamarina, J.C., Ruppel, C., 2005. Compressional and shear wave velocities in uncemented sediment containing gas hydrate. Geophysical Research Letters 32 (10), L10609. doi:10.1029/2005GL022607.

Yun, T.S., Ruppel, C., Santamarina, J.C., 2007. Mechanical properties of sand, silt, and clay containing tetrahydrofuran hydrate. Journal of Geophysical Research 112, B04106. doi:10.1029/2006JB004484.

Please cite this article as: Ellis, S., et al., Testing proposed mechanisms for seafloor weakening at the top of gas hydrate stability on an uplifted submarine ridge (Rock Garden), New Zealand, Marine Geology (2009), doi:10.1016/j.margeo.2009.10.008